BULLETIN OF THE POLISH ACADEMY OF SCIENCES
TECHNICAL SCIENCES, Vol. 71(4), 2023, Article number: e145936
DOI: 10.24425/bpasts.2023.145936

Manufacturing of thin-walled, complex polymer parts by DLP printing – the influence of process parameters on the crosslinking density

Dorota TOMCZAK[1]*, **Radosław WICHNIAREK**[2], **Wiesław KUCZKO**[2], **and Filip GÓRSKI**[2]

[1] Institute of Chemical Technology and Engineering, Poznan University of Technology, Berdychowo 4, 60-965 Poznan, Poland
[2] Faculty of Mechanical Engineering, Poznan University of Technology, Piotrowo 3, 61-138 Poznan, Poland

Abstract. This study investigated the relationship between the parameters of the DLP manufacturing process and the structure of photopolymerizable acrylic resins. Four different process parameters were established to produce different thin-walled acrylic sample series: exposure time, layer thickness, area offset, and number of transition layers. The structure and the surface of the obtained samples were examined with the use of the FTIR–ATR method and an optical microscope, respectively. It was proved that extension of the exposure time increases the density of crosslinking and sample thickness. A decreasing crosslinking density due to rising layer thickness is observed. The area offset affects only the dimensions of the sample, predictably reducing the dimensions of the sample as the compensation increases. The absence of transition layers proved unfavorable in many respects, both structurally and geometrically.

Key words: Additive manufacturing; DLP; acrylic resin; crosslinking density; FTIR–ATR.

1. INTRODUCTION

Currently, rising consumer expectations for the quality and comfort of life require the production of multifunctional and complex products that are convenient to use. To meet such expectations, it is often necessary to miniaturize products, which are common in all areas of life [1–3]. The trend toward miniaturization can especially be seen in the electronics industry [4–6]. In systems made up of very small parts, special attention should be paid to the dimensional accuracy of the parts to ensure long-term cooperation. One of the important types of parts are thin-walled parts in which one of the dimensions does not exceed 1–2 mm [2, 7]. Because of their small dimensions, the production of thin-walled products using conventional methods is a challenge due to many defects that can occur in the final parts, such as nonconformity of the product geometry, insufficient strength properties, warpings, and welding lines [7–9]. Even with additive manufacturing, not all methods facilitate the precise production of small parts, especially those with complex shapes [10]. One of the methods that avoid most of these problems and obtain complex thin-walled parts is Digital Light Processing, customarily called DLP printing [11,12]. DLP is an additive manufacturing technique, where high-resolution light engines are used to cure a thin layer of the material with a precision of less than 100 micrometers [13]. This method is used to obtain complex and detailed parts made from each engineering material, such as ceramics [14], metals [15], or polymers [16]. The first two are mainly used to obtain composites with polymer matrix [14,17,18]. Therefore, the most important group of materials used in DLP printing is photocurable polymers. During the printing process, a beam of UV light is projected onto the polymer layer to cure it in one exposure. Curing occurs through activation of the photopolymerization reaction [19–21]. For the DLP printing process, the most common photopolymerizable resins used are epoxy and acrylic resins; however, there is ongoing work to introduce alternatives to polymers obtained from non-renewable resources [22, 23]. Polyacrylates belong to the most interesting photocurable polymers. Due to their specific properties, they find application in many industries [24], such as pharmaceutical [25], automotive [26], and microelectronics [27]. Certain types of products, such as microneedles with drug content, require the use of very fine geometries [28, 29]. Moreover, the content of expensive additives (e.g., drugs) doped into the photocurable resin induces the need to minimize the total amount of mixed material throughout the DLP process, which was the authors' motivation to evaluate the smallest amount of resin necessary to print the designed samples.

Structures formed in acrylic parts have a characterizing parameter called crosslinked density, which is related to crosslinked structure in polyacrylates that results from a linking of the monomers due to the double bond conversion (DC) [30–32]. The crosslinking density specified by the DC rate is expressed by the segments of polymer chain density that connect two parts of the polymer net [33]. The crosslinking density influences the vast majority of properties of the photocurable resin part, such as mechanical parameters (tensile strength, hardness, impact strength) or physicochemical parameters (characteristic temper-

*e-mail: dorota.tomczak@doctorate.put.poznan.pl

Manuscript submitted 2022-12-19, revised 2023-02-24, initially accepted for publication 2023-04-30, published in August 2023.

atures, thermal stability, flame retardancy, viscosity). The proof of this is several studies that determined the crosslinking density to assess its impact degree on the performance properties of the material. In [34] Memon H. *et al*. studied the correlation between the thermal and mechanical properties of a novel epoxy vitrimer resin and its crosslinking density. The results showed that a decrease in the crosslinking density entails a reduction in the tensile strength and Young's modulus values, and surprisingly, an increase in strength retention efficiency. Thermal properties such as the temperature of degradation and percentage of charring improved after raising the crosslinking density. Similarly, Y. Du *et al*. in [16] proved that the value of crosslinking density is connected proportionally to the thermal stability, flame retardancy, and impact strength under the condition that the critical value is not exceeded by the crosslinking density. Above this value, properties will deteriorate. Yu J.W. *et al*. [35] concluded that the glass transition temperature and tensile strength of epoxy resin, functionalized by graphene oxide co-curing agents, is improved with an increase in crosslinking density. Their results confirmed this claim for the studied natural flavonoid-based epoxy resins. Lesser J.A. [36] proved that the overall resistance to damage and residual compressive strength of epoxy resin-based composites steadily grow as crosslinking density increases. Meng J. *et al*. [37] developed a multilayer tubular microstructure with high crosslinking density, which resulted in improved mechanical properties and provides strong fire resistance without flame retardants in bio-based furan epoxy resins. Bandyopadhyay A. *et al*. [38] conducted a simulation on the molecular dynamics and mechanics of epoxy polymers. The results clearly showed the glass transition temperature growth, enhancement of the elastic properties, and decrease in the thermal expansion coefficient with increasing crosslinking density. Choi J.H. *et al*. [18] worked on developing a heat-conductive epoxide material with carbon nanotubes. Interestingly, they found that the density of crosslinking affected positively or negatively the conductivity depending on the content of nanotubes in the resin structure. Hu K. *et al*. [39] confirmed that the growth of crosslinking density has a positive effect on tensile strength and reduces the elongation break, increasing the viscosity of the acrylic resin.

In order to receive the material with the designated degree of crosslinking by using the DLP method, it is necessary to choose the optimal process parameters. Finding the relation between parameters and properties of a final product was an important aspect for the authors. The influence of the printed layer thickness on mechanical properties, especially the flexural strength of dental acrylic resin and composite material consisting of ZrO_2 and ATZ, were studied in [40] and [41]. Furthermore, Seprianto D. *et al*. [42] proved that layer thickness is the main parameter that influences impact strength of the samples made from UV Resin Anycubic material. Saed A.B. *et al*. [43] studied the influence of dye concentration and exposure time on dimensional inaccuracy, porosity and compressive strength of poly-L-lactic acid samples. They showed that as exposure time increased, the samples were more geometrically accurate, less porous, and more resistant to compression. Furthermore, Qi G. *et al*. [44] proved that the curing depth of the porous acrylic-based ceramic samples increases with the exposure time increase. Guerra A.J. *et al*. [20] claimed that resin parts have a strong influence on cure depth of printed parts, as well as exposure time, which in general induces the growth of the cure depth with the time extension. The postprocessing curing influence on mechanical and thermal properties of acrylic dental parts was investigated by Redutko J.*et al*. [45]. They showed that there is an optimal time of post-curing for a particular resin. Shen M. *et al*. [46] and Hanon M.M. *et al*. [47] carried out a study regarding the printing angle influence on mechanical properties, such as flexural strength or dynamic coefficient of friction of resin-based ceramic composite parts. The results showed that samples printed at a printing angle of 45° have the lowest flexural strength and lower dynamic coefficient of friction values. In the study [48] Du Y. *et al*. showed that different types of photoinitiators make different thicknesses of cured layers in hydroxyapatite-acrylic scaffolds possible. Moreover, the exposure time extension resulted in the rise of the layer thickness value.

As can be seen, a lot of effort goes into research regarding the effect of the DLP process parameters and the crosslinking density on the properties of various materials. However, only a few publications referenced in this study were related to acrylic resins. The majority of these publications are related to materials based on epoxy resins. To the best of the authors' knowledge, there are no studies where the connection between DLP printing process parameters and the material structure, especially acrylic resin, was discussed. Obtained results will be useful in predicting material properties obtained by DLP, and could potentially reduce the need for destructive tests, such as tensile testing and impact testing. This study shows the influence of curing time, layer thickness, area offset and the number of transition layers on the crosslinking density of photocurable acrylic resin during the production of thin-wall parts in the DLP printing process. The goal was to minimize the use of non-renewable polymers to increase the method application potential in the industry. The novelty of this study includes the use of one of the most modern types of printing machine, the Phrozen Sonic Mini 8K, with high printing resolution on the order of 22 μm [49]. Phrozen equipment is also in use by other researchers [50], which could help to implement the DLP printing method as a means of obtaining reproducible, high-quality parts in the future.

2. MATERIALS AND METHODS

2.1. Materials

Acrylic, photocurable Phrozen Aqua Gray 8K Resin (Phrozen Technology, Taiwan) was used in this study. Its properties are shown in Table 1. The resin consists of the following monomers and additives: urethane acrylate, dipropylene glycol diacrylate (DPGDA), epoxy acrylate, acryloyl morpholine, tris (2–hydroxy ethyl) isocyanurate triacrylate (TIT), diphenyl (2,4,6–trimethyl benzoyl) phosphine oxide (TPO), silicon dioxide, titanium dioxide, and carbon black [49]. The quantities of each part were not made available by the manufacturer except for TPO – 1–10%, TiO_2 – $< 1\%$ and C – $< 1\%$.

Table 1
Chemical and physical properties of Phrozen Aqua Gray 8K Resin [49]

Property	Values
Appearance and color	Gray viscous liquid
Flash point	$> 110°C/230°F$
Specific gravity	1.18 g/cm^3 at 25°C/77°F
Viscosity	320–350 cps
Solubility in water	Insoluble
Organic solvents solubility	Soluble
Electric conductivity	Dielectric

2.2. Sample preparation

The 31 rectangular samples were made from acrylic resin and characterized by dimensions of $10 \times 8 \times 1$ mm. One corner was chamfered to allow evaluation of visual aspects and the repeatability of the printing process. The sample drawing can be seen in Fig. 1. The designed part does not have supports, which because of its small dimensions and easy geometry, is preferred in the DLP process. After printing, the samples were cleaned in alcohol.

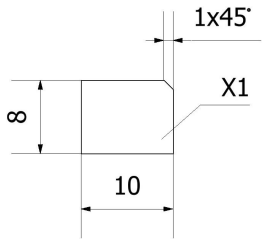

Fig. 1. Sample drawing

2.3. Methods

A Phrozen Sonic Mini 8K printer was used in this study. To prepare the printing process, including setting the process parameters, Chitubox PRO (CHITUBOX, China) software was used. The base parameters of the printing process are shown in Table 2.

2.4. Measurement and characterization

To determine the crosslinking density of specimens by DC ratio, the Jasco FT/IR–4600 spectrometer was used. During FTIR–ATR measurements, the surface of the sample that adhered to the working table was tested due to its better surface quality. The process was carried out with parameters including 64 scans, a resolution of 2 cm^{-1}, and in the range of 4000–400 cm^{-1}. The percentage of acrylic double bond (C=C) conversion was calculated by equation (1):

$$DC\ (\%) = \frac{(A_{1407}/A_{1722})_0 - (A_{1407}/A_{1722})_t}{(A_{1407}/A_{1722})_0} \times 100, \quad (1)$$

where $(A_{1407}/A_{1722})_0$ and $(A_{1407}/A_{1722})_t$ are relative absorbance (peak–area ratio) of double bonds in the structure before curing and after curing in a given t time [30–32].

Table 2
Base printing parameters

Parameter	Value
Layer height	0.03 mm
Bottom exposure time	35 s
Transition layer count (TL)	6
Bottom layer count	6
Exposure time	2 s
Transition type	linear
Rest time before lift	0 s
Rest time after lift	0 s
Rest time after retract	4 s
Bottom lift distance	6 mm
Lifting distance	6 mm
Bottom lift speed	150 mm/min
Bottom retract speed	150 mm/min

The Insize ISM-PM200SB microscope with magnification of 245×, a micrometer and caliper were used to examine the surface and dimensions of the samples.

3. RESULTS AND DISCUSSION

The samples obtained in this study were manufactured using a model with dimensions of $10 \times 8 \times 1$ mm with an accuracy of 0.05 mm. To check how much resin is needed to produce a sample, in the beginning, the amount of resin in the resin tank was 3 ml. At this amount, 9 samples were obtained without changing parameters; however, defects were found in the 10th sample, which indicates too little resin was in the resin tank (unprinted layers). When 2 ml of resin was used, a second sample in the series could not be obtained. The activities described indicate there is no need to cover the whole area of the resin tank bottom to make parts with small dimensions.

3.1. Structure analysis

The composition of the acrylic resin, except for C, SiO_2 and TiO_2 is shown in Fig. 2. The urethane acrylate was the main acrylic monomer, while DPGDA and epoxy acrylate acted as the crosslinking agents. The acryloyl morpholine and the tris (2–hydroxy ethyl) isocyanurate triacrylate were solvents. The TPO was an initiator of photopolymerization of the resin by the radical system mechanism due to breaking of the bond between carbon and phosphorus in the compounds under UV light. The resulting radicals started a series of chemical reactions that caused the crosslinking of acrylic monomers and crosslinking compounds, facilitating the formation of a highly crosslinked structure. The remaining compounds, such as SiO_2, TiO_2, and C, did not take part in the photopolymerization process, but acted as a coloring agent, stabilizer, and opacifier.

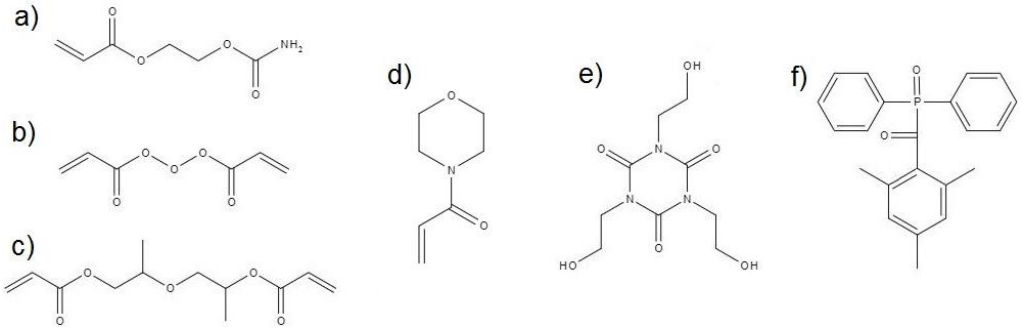

Fig. 2. Molecular structure of the compounds: a) urethane acrylate, and photoinitiator f) TPO. b) epoxy acrylate, c) DPGDA, d) acryloyl morpholine, e) TIT

The FTIR–ATR spectrums of the uncrosslinked and crosslinked resin are presented in Fig. 3. The characteristic absorption bands of (–OH), (C=O), and (C=C) bonds were specified based on [30] and [51–54]. According to studies, the bands at 1644, 1407, 808, and one at 1612 cm^{-1} are related to aliphatic (acrylic) and aromatic double bonds, respectively. The intensity of the aliphatic bands decreased after the crosslinking process confirmed the photopolymerization process occurrence. The absorption band at 763 (for uncrosslinked resin), 1635, and the wide band observed at 3000–3600 cm^{-1} are characteristic of the (–OH) functional group [54, 55]. For uncrosslinked resin current (–OH) groups are related to TIT presence, while for the crosslinked sample they are also connected to the appearance of emerged water trapped in the structure of resin or new chemical compounds formed as a result of intensified contact of resin with oxygen from the air by too small amount of the resin in the resin tank. The inhibition of photopolymerization caused by oxygen, and the emerging compounds were studied in [56–58]. However, Zhang L. *et al*. [59] proved that oxygen can be a catalyst of photopolymerization, which is why influence of oxygen on the polymerization process induced by UV light is still unexplored, especially for the complex chemical composition of the resin; therefore, more research is needed in this area.

Equation (1) characterizes how many of the double bonds present in the acrylic monomers and crosslinking compounds have converted, which illustrates the degree of crosslinking of the resin. The peak areas associated with (=CH2) acrylic bonds needed to be used in the calculations. In these studies, due to the changing bandwidths for 1644 and 808 cm^{-1} caused by the presence of the (–OH) band at 1635 and 791 cm^{-1}, the band areas for 1407 cm^{-1} were used in the calculations. The (C=O) band at 1722 cm^{-1} was used as the internal standard.

Figure 4 shows the values of crosslinking density in each successive sample with attention to the moments of change of a given parameter (layer thickness, exposure time of bottom layers, number of transition layers, and area offset). As can be seen for the first 14 samples, the DC values fluctuate sinusoidally and approach the average value of 87±2%. The reduction of DC values was a result of the layer thickness increase, which can be caused by the difficulty in crosslinking the printed layer top. Furthermore, the carbon and TiO_2 which absorb the UV light could be a barrier.

Shortening the exposure time to 8 s significantly reduced the DC value, which increased back for the following samples. Therefore, a parameter change caused a temporary destabilization of the process. The higher value of DC was reached for 35 s

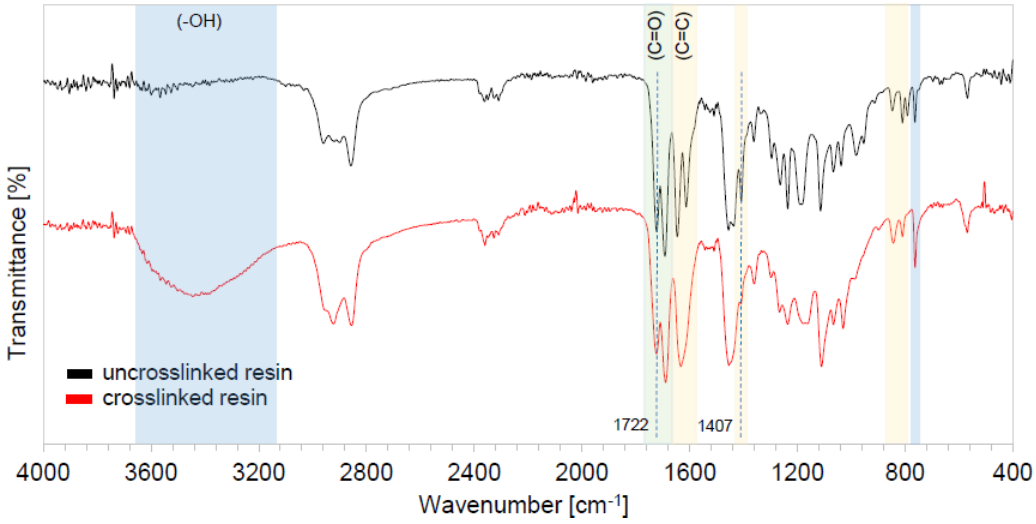

Fig. 3. FTIR–ATR spectrum for uncrosslinked and crosslinked resin (sample 3) [30, 50–53]

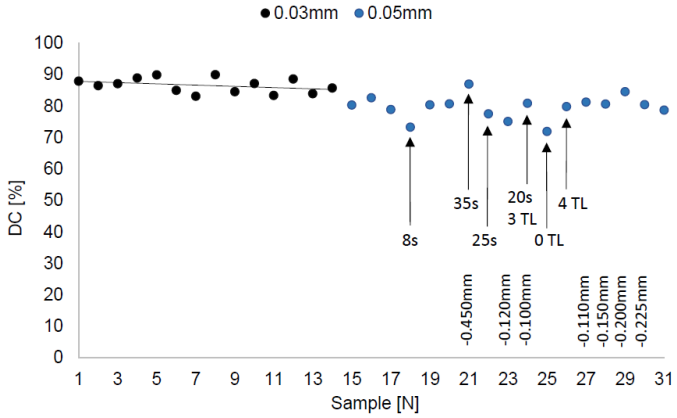

Fig. 4. Crosslinking density of the sample depending on the thickness of the printed layer (0.03 or 0.05 mm), bottom layer cure time (8, 20, 25, 35 s), number of transition layers (0, 3, 4 TL) and value of area offset (0.100–0.450 mm)

exposure time, which is in accordance with the manufacturer's recommendations. When the exposure is shorter, for instance, 20 or 25 s, the structure is less crosslinked.

The absence of the transition layers caused a notable reduction in DC value, which was a result of testing the top layers of the sample in the FTIR–ATR test, which had a much shorter crosslinking time (2 s) than the bottom layers. This is confirmed by an additional measurement carried out by the authors, in which for the sample tested by the surface of the working table (bottom layers), DC was 85%, and 71% by the side of the resin tank (top layers). Therefore, the samples differ in properties at thickness. The change in the area offset of the bottom layers did not affect the crosslinking density.

3.2. Dimensional and visual analysis

The dependence of sample thickness on parameters for individual samples is shown in Fig. 5. No relationship between sample thickness and crosslinking density can be observed. The sample thickness rose and stabilized for the first 9 samples,

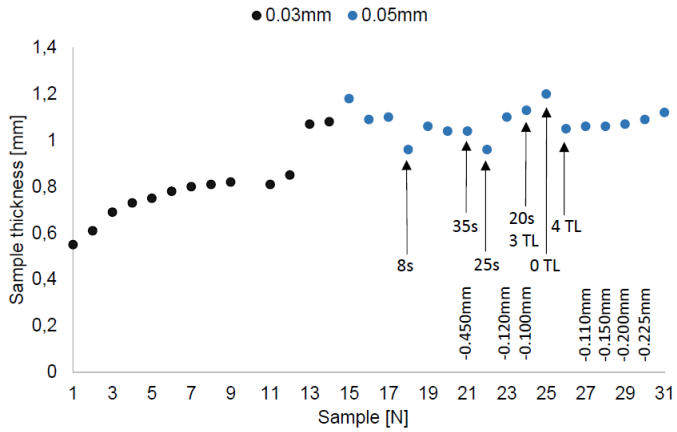

Fig. 5. Thickness of the sample depending on the thickness of the printed layer (0.03 or 0.05 mm), bottom layer cure time (8, 20, 25, 35 s), number of transition layers (0, 3, 4 TL) and value of area offset (0.100–0.450 mm)

and reached the value of 0.82 mm, which is not within the assumed dimensional accuracy. The value of sample thickness of 1.07 mm can be noticed for sample 13, which resulted from the use of a coarser gauge (0.33 mm instead of 0.11 mm) for calibration. The change in printed layer thickness induced a jump in the thickness value to 1.18 mm, which then decreased to 1.09 and 1.1 mm for the 16th and 17th samples, respectively. Again, a parameter change caused a process destabilization. When the exposure time was extended, there were non-characteristic changes in sample thickness caused by a simultaneous change of the area offset of 0.45 mm for dimensions in the OX and OY axes, which also influenced dimensions in the OZ axis. Therefore, the increase in the crosslinking time seemingly did not affect the thickness of the sample. Due to parameter changes, it can be observed that decrease in the crosslinking time for samples 21 and 22 reduced the thickness of the sample, while the rise of the compensation for samples 22 and 23 decreased the thickness and other dimensions of the sample. The absence of transition layers caused the sample thickness to increase to 1.2 mm, which is undesirable. For samples 26 to 31, a rise in the sample thickness can be noticed, just like for samples 1–9; however, due to the compensation used, it has a slightly different character. The growth in the value of compensation caused a decline in thickness; however, the unexplained increase in sample thickness with each printed part caused the thickness value to be almost constant instead of decreasing.

Figure 6 shows the effect of increasing the compensation of bottom layer dimensions on their geometry. The a and b images clearly show the larger dimensions of the bottom layers (right side) in comparison to the top layers (left side) of the sample. When the compensation was increased from 0.100 to 0.225 mm (photos from a to d), a $10 \times 8 \times 1$ mm sample was obtained,

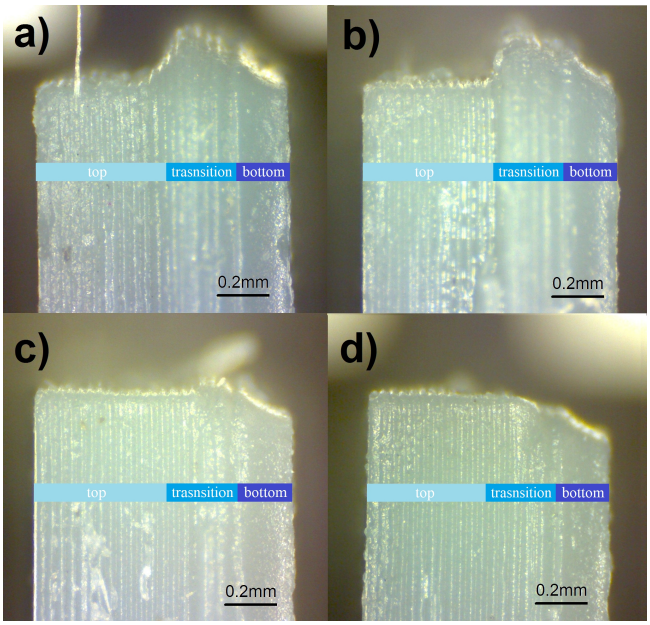

Fig. 6. Images of sample a) 23. with area offset of –0.120 mm, b) 25. with area offset of –0.100 mm, c) 28. with area offset of –0.150 mm and d) 30. with area offset of –0.225 mm and with marked top, transition and bottom printed layers

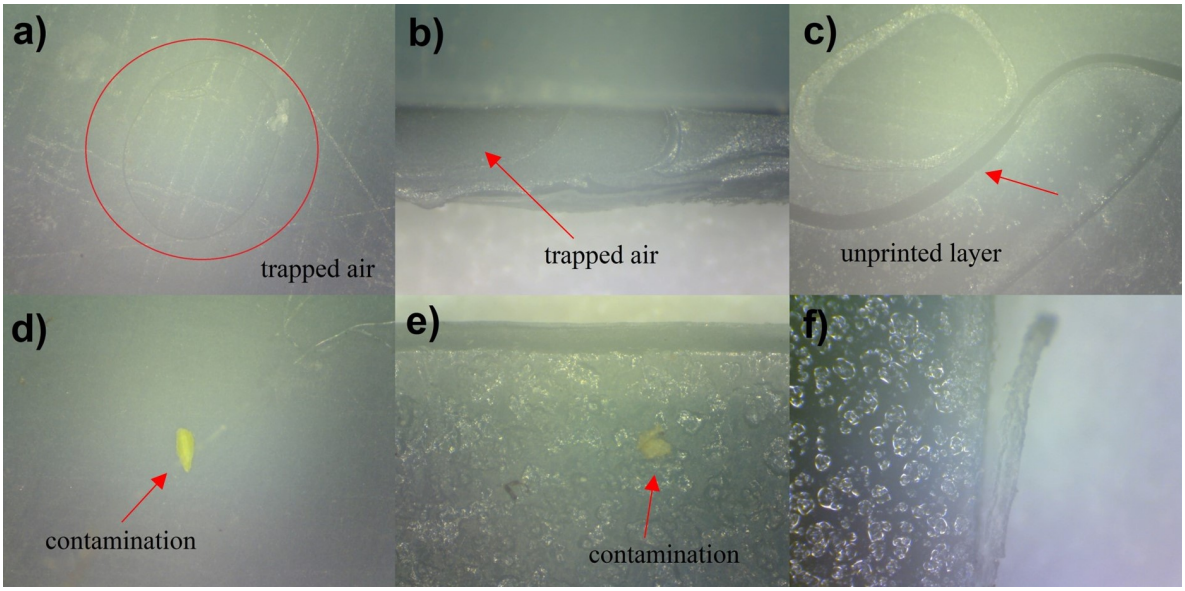

Fig. 7. Selected images of surface of printed samples

which was the authors' goal. It was not possible to eliminate the growth of the dimensions of the bottom layers with each successive printed layer, which can be seen as a bevel. Based on Fig. 6b, it can be concluded that for sample 25 with no transition layers, bottom layers were printed instead of transition layers, which turned out to be highly unfavorable for both geometric and practical reasons – a step change in the structure of the sample induces a step change in properties, which can result in faster destruction of the sample (e.g., delamination).

Figure 7 shows microscope photos of various defects appearing in samples printed by DLP. Trapped air and unprinted layers are shown in images a, b and c. Various types of inclusions (fibers, microparticles) are shown in d and e. The f photo shows the effect of light scattering, which can be caused by bleeding pixels or the photopolymer itself [29]. Some of the listed defects can be prevented by parameter changes or more attentive actions by the authors; however, some defects should be fixed by the manufacturers of the software or the printing device. This represents a broad field of research.

4. CONCLUSIONS

The DLP printing process made it possible to produce thin-walled acrylic samples with expected geometric parameters. This study has an indicative nature because of too few samples affecting the relevance of inference for changing the process parameters. However, some conclusions can be drawn, including that with shorter exposure time, less structure is crosslinked. For the studied acrylic resin, the threshold was 35 s. Furthermore, rising values of printed layer thickness caused a decrease in the DC value. Shortening of the exposure time and enlarging of the area offset resulted in the decline of the sample thickness.

For both crosslinking density and thickness of the sample, any change in parameters caused a temporary destabilization of the printing process.

The sample thickness increase with each printed sample without changing the parameters can be observed. Furthermore, undesirable compounds containing (–OH) functional groups were detected in the printed sample structure. Further research is needed to determine the cause and eliminate the process defects.

The DLP process has great potential for implementation in many industrial applications where small and precise parts need to be produced, it seems to be almost wasteless, and is a relatively fast and low-cost manufacturing process. There is still much to be explored in this area. This is especially true for acrylic photopolymer materials that are doped with additives.

ACKNOWLEDGEMENTS

This research was funded by statutory activity financed by the Polish Ministry of Science and Higher Education, grant number (0613/SBAD/4770).

REFERENCES

[1] S. Mcnair *et al.*, "Manufacturing technologies and joining methods of metallic thin-walled pipes for use in high pressure cooling systems," *Int. J. Adv. Manuf. Technol.*, vol. 118, pp. 667–681, 2022, doi: 10.1007/s00170-021-07982-8.

[2] C. Kailasanathan, S. Saravanan, E. Natarajan, and B. Stalin, "Polyoxymethylene/talc composite: Investigation of warpage, mechanical and thermal properties for thin walled-injection molding applications," *J. Appl. Polym. Sci.*, vol. 139, pp. e51762-1–e51762-12, 2022, doi: 10.1002/app.51762.

[3] A. Ornat, M. Uliasz, G. Bomba, A. Burghardt, K. Kurc, and D. Szybicki, "Robotised Geometric Inspection of Thin-Walled Aerospace Casings," *Sensors*, vol. 22, pp. 3457-1–3457-17, 2022, doi: 10.3390/s22093457.

[4] P. Muszyński, P. Poszwa, A. Gessner, and K. Mrozek, "Application of Selective Induction Heating for Improvement of Mechanical Properties of Elastic Hinges," *Materials*, vol. 14, pp. 2543-1–2543-13, 2021, doi: 10.3390/ma14102543.

[5] X. Wang *et al.*, "Electrospun Thin-Walled CuCo2O4@C Nanotubes as Bifunctional Oxygen Electrocatalysts for Rechargeable Zn−Air Batteries," *Nano Lett.*, vol. 17, pp. 7989–7994, 2017, doi: 10.1021/acs.nanolett.7b04502.

[6] R. Kulkarni *et al.*, "An Assessment of Thermoset Injection Molding for Thin-WalledConformal Encapsulation of Board-Level Electronic Packages," *J. Manuf. Mater. Process.*, vol. 3, pp. 18-1–18-16, 2019, doi: 10.3390/jmmp3010018.

[7] K. Mrozek and S. Chen, "Selective induction heating to eliminate the fundamental defects of thin-walled moldings used in electrical industry," *J. Appl. Polym. Sci.*, vol. 44992, pp. 44992-1–44992-17, 2017, doi: 10.1002/APP.44992.

[8] S. Nian, C. Wu, and M. Huang, "Warpage control of thin-walled injection molding using local mold temperatures," *Int. Commun. Heat Mass Transf.*, vol. 61, pp. 102–110, 2015, doi: 10.1016/j.icheatmasstransfer.2014.12.008.

[9] Q. Feng, L. Liu and X. Zhou, "Automated multi-objective optimization for thin-walled plastic products using Taguchi, ANOVA, and hybrid ANN-MOGA," *Int. J. Adv. Manuf. Technol.*, vol. 106, pp. 559575, 2020, doi: 10.1007/s00170-019-04488-2.

[10] W. Kuczko, A. Hamrol, R. Wichniarek, F. Górski, and M. Rogalewicz, "Mechanical properties and geometric accuracy of angle-shaped parts manufactured using the FFF method," *Bull. Pol. Acad. Sci.-Tech. Sci.*, vol. 69, no. 3, pp. e137387-1–e1317387-9, 2021, doi: 10.24425/bpasts.2021.137387.

[11] S. Gao, C. Wang, B. Xing, M. Shen, W. Zhao, and Z. Zhao, "Experimental investigation on bending behaviour of ZrO_2 honeycomb sandwich structures prepared by DLP stereolitography," *Thin-Walled Struct.*, vol. 157, pp. 107099-1–107099-12, 2020, doi: 10.1016/j.tws.2020.107099.

[12] S. Li, M. Hu, L. Xiao, and W. Song, "Compressive properties and collapse behavior of additively-manufactured layered-hybrid lattice structures under static and dynamic loadings," *Thin-Walled Struct.*, vol. 157, pp. 107153-1–107153-22, 2020, doi: 10.1016/j.tws.2020.107153.

[13] M. Lebedevaite, V. Talacka, and J. Ostrauskaite, "High biorenewable content acrylate photocurable resins for DLP 3D printing," *J. Appl. Polym. Sci.*, vol. 138, pp. 1–13, 2020, doi: 10.1002/app.50233.

[14] G. Qi, Y. Zeng, and J. Chen, "Preparation of porous SnO_2-based ceramics with lattice structure by DLP," *Ceram. Int.*, vol. 48, pp. 14568–14577, 2022, doi: 10.1016/j.ceramint.2022.01.350.

[15] M. Gregorini, R. Grass, and W. Stark, "One-Step Photolithographic Surface Patterning of Nanometer-Thick Gold Surfaces by Using a Commercial DLP Projector and the Fabrication of a Microheater," *Ind. Eng. Chem. Res.*, vol. 59, pp. 12048–12055, 2020, doi: 10.1021/acs.iecr.9b05837.

[16] Y. Du, G. Zhao, G. Shi, Y. Wang, W. Li, and S. Ren, "Effect of crosslink structure on mechanical properties, thermal stability and flame retardancy of natural flavonoid based epoxy resins," *Eur. Polym. J.*, vol. 162, pp. 110898-1–110898-8, 2022, doi: 10.1016/j.eurpolymj.2021.110898.

[17] S. Tsai, L. Chen, C. Chu, W. Chao, and Y. Liao, "Photo curable resin for 3D printed conductive structures," *Addit. Manuf.*, vol. 51, pp. 102590-1–102590-8, 2022, doi: 10.1016/j.addma.2021.102590.

[18] J. Choi, H. Song, J. Jung, J. Yu, N. You, and M. Goh, "Effect of crosslink density on thermal conductivity of epoxy/carbon nanotube nanocomposites," *J. Appl. Polym. Sci.*, vol. 44253 pp. 1–7, 2017, doi: 10.1002/APP.44253.

[19] Y. Li, Q. Mao, J. Yin, Y. Wang, J. Fu, and Y. Huang, "Theoretical prediction and experimental validation of the digital light processing (DLP) working curve for photocurable materials," *Addit. Manuf.*, vol. 37, pp. 101716-1–101716-10, 2021, doi: 10.1016/j.addma.2020.101716.

[20] A. Guerra *et al.*, "Optimisation of photocrosslinkable resin components and 3D printing process parameters," *Acta Biomater.*, vol. 97, pp. 154–161, 2019, doi: 10.1016/j.actbio.2019.07.045.

[21] A. Bagheri and J. Jin, "Photopolymerization in 3D Printing," *ACS Appl. Polym. Mater.*, vol. 1, pp. 593–611, 2019, doi: 10.1021/acsapm.8b00165.

[22] C. Noè *et al.*, "DLP-printable fully biobased soybean oil composites," *Polymer*, vol. 247, pp. 124779-1–124779-9, 2022, doi: 10.1016/j.polymer.2022.124779.

[23] M. Lebedevaite, V. Talacka, and J. Ostrauskaite, "High biorenewable content acrylate photocurable resins for DLP 3D printing," *J. Appl. Sci.*, vol. 138, pp. e50233-1–e50233-13, 2021, doi: 10.1002/app.50233.

[24] D. Patel, A. Sakhaei, M. Layani, B. Zhang, Q. Ge, and S. Magdassi, "Highly Stretchable and UV Curable Elastomers for Digital Light Processing Based 3D Printing," *Adv. Mater.*, vol. 29, no. 15, p. 1606000, 2017, doi: 10.1002/adma.201606000.

[25] G. Yang, M. He, S. Zhang, M. Wu, and Y. Gao, "An acryl resin-based swellable microneedles for controlled release intradermal delivery of granisetron," *Drug Dev. Ind. Pharm.*, vol. 44, pp. 808–816, 2018, doi: 10.1080/03639045.2017.1414230.

[26] X. Zijie, L. Chao, X. Guilong, and H. Jian, "Modification of polyacrylate resin to prepare water-soluble poly-epoxy-acrylate resin for its application as an automotive oil filter paper binder," *J. Vinyl Addit. Technol.*, vol. 27, pp. 833–840, 2021, doi: 10.1002/vnl.21854.

[27] Y. Dou, F. Li, B. Tang, and G. Zhou, "Surface Wettability Tuning of Acrylic Resin Photoresist and Its Aging Performance," *Sensors*, vol. 21, no. 14, pp. 4866-1–4866-11, 2021, doi: 10.3390/s21144866.

[28] A. Ghavami-Nejad *et al.*, "Glucose-Responsive Composite Microneedle Patch for Hypoglycemia-Triggered Delivery of Native Glucagon," *Adv. Mater.*, vol. 31, pp. 1901051-1–1901051-7, 2019, doi: 10.1002/adma.201901051.

[29] A. Kundu *et al.*, "DLP 3D Printed "Intelligent" Microneedle Array (iμNA) for Stimuli Responsive Release of Drugs and Its in Vitro and ex Vivo Characterization," *J. Microelectromech. Syst.*, vol. 29, no. 5, pp. 685–691, 2020, doi: 10.1109/JMEMS.2020.3003628.

[30] Q. Luo *et al.*, "Preparation and Properties of Novel Modi?ed Waterborne Polyurethane Acrylate," *Coatings*, vol. 12, pp. 1135-1–1135-14, 2022, doi: 10.3390/coatings12081135.

[31] D. Kunwong, N. Sumanochitrapom, and S. Kaewpirom, "Curing behavior of a UV-curable coating based on urethane acrylate oligomer: the influence of reactive monomers," *Songklanakarin J. Technol.*, vol. 33, no. 2, pp. 201–207, 2011.

[32] H. Xiang *et al.*, "Preparation, Characterization and Application of UV-Curable Flexible Hyperbranched Polyurethane Acrylate," *Polymers*, vol. 9, pp. 552-1–552-12, 2017, doi: 10.3390/polym9110552.

[33] R. Wool, "7 – Properties of Triglyceride-Based Thermosets," in *Bio-Based Polymers and Composites*, 1st ed., R. Wool and X. Sun, Eds. Elsevier Academic Press, 2005, pp. 202-225.

[34] H. Memon, Y. Wei, and C. Zhu, "Correlating the thermomechanical properties of a novel bio-based epoxy vitrimer with its crosslink density," *Mater. Today Commun.*, vol. 29, pp. 102814-1–102814-7, 2021, doi: 10.1016/j.mtcomm.2021.102814.

[35] J. Yu *et al.*, "Enhancement of the crosslink density, glass transition temperature, and strength of epoxy resin by using functionalized graphene oxide co-curing agents," *Polym. Chem.*, vol. 7, pp. 36–43, 2016, doi: 10.1039/C5PY01483B.

[36] A. Lesser, "Effect of Resin Crosslink Density on the Impact Damage Resistance of Laminated Composites," *Polym. Compos.*, vol. 18, pp. 16–27, 1997, doi: 10.1002/pc.10257.

[37] J. Meng *et al.*, "Flame Retardancy and Mechanical Properties of Bio-Based Furan Epoxy Resins with High Crosslink Density," *Macromol. Mater. Eng.*, vol. 305, pp. 1900587-1–1900587-8, 2020, doi: 10.1002/mame.201900587.

[38] A. Bandyopadhyay, P. Valavala, T. Clancy, K. Wise, and G. Odegard, "Molecular modeling of crosslinked epoxy polymers: The effect of crosslink density on thermomechanical properties," *Polymer*, vol. 52, no. 11, pp. 2445–2452, 2011, doi: 10.1016/j.polymer.2011.03.052.

[39] K. Hu, W. Kong, X. Fu, C. Zhou, and J. Lei, "Resistivity optimization and properties of silver nanoparticles-filled alcohol-soluble conductive coating based on acrylic resin," *High Perform. Polym.*, vol. 27, pp. 8-1–8-9, 2015, doi: 10.1177/0954008314566433.

[40] A. Alshamrani, R. Raju, and A. Ellakwa, "Effect of Printing Layer Thickness and Postprinting Conditions on the Flexural Strength and Hardness of a 3D-Printed Resin," *Biomed Res. Int.*, vol. 2022, pp. 8353137-1–8353137-9, 2022, doi: 10.1155/2022/8353137.

[41] M. Borlaf, L. Conti, and T. Graule, "Influence of tensile edge design and printing parameters on the flexural strength of ZrO_2 and ATZ bars prepared by UV-LCM-DLP," *Open Ceram.*, vol. 5, pp. 100066-1–10006-5, 2021, doi: 10.1016/j.oceram.2021.100066.

[42] D. Seprianto, R. Sugiantoro, Sipironi, Yahya and M. Erwin, "The Effect of Rectangular Parallel Key Manufacturing Process Parameters Made with Stereolithography DLP 3D Printer Technology Against Impact Strength," *J. Phys.-Conf. Ser.*, vol. 1500, pp. 012028-7–012028-7, 2020, doi: 10.1088/1742-6596/1500/1/012028.

[43] A. Saed, A. Behravesh, S. Hasannia, S. Ardebili, B. Akhoundi, and M. Pourghayoumi, "Functionalized poly-L-lactic acid synthesis and optimization of process parameters for 3D printing of porous sca?olds via digital light processing (DLP) method," *J. Manuf. Process.*, vol. 56, pp. 550–561, 2020, doi: 10.1016/j.jmapro.2020.04.076.

[44] G. Qi, Y. Zeng, and J. Chen, "Preparation of porous SnO_2-based ceramics with lattice structure by DLP," *Ceram Int.*, vol. 48, pp. 14568–14577, 2022, doi: 10.1016/j.ceramint.2022.01.350.

[45] J. Redutko, A. Kalwik, and A. Szarek, "Influence of Curing Time on Properties of Dental Photosensitive Resin Applied in DLP Technique of 3D Printing," *Arch. Metall. Mater.*, vol. 66, no. 2, pp. 419–424, 2021, doi: 10.24425/amm.2021.135873.

[46] M. Shen *et al.*, "Effects of exposure time and printing angle on the curing characteristics and flexural strength of ceramic samples fabricated via digital light processing," *Ceram. Int.*, vol. 46, no. 15, pp. 24379–24384, 2020, doi: 10.1016/j.ceramint.2020.06.220.

[47] M. Hanon, A. Ghaly, L. Zsidai, and S. Klébert, "Tribological characteristics of digital light processing (DLP) 3D printed graphene/resin composite: Influence of graphene presence and process settings," *Mater. Des.*, vol. 218, pp. 110718-1–110718-17, 2022, doi: 10.1016/j.matdes.2022.110718.

[48] Y. Du, T. Hu, J. You, Y. Ye, B. Zhang, B. Bao, M. Li, Y. Liu, Y. Wang, and T. Wang, "Study off alling-down-type DLP 3D printing technology for high-resolution hydroxyapatite scaffolds," *Intl. J. Appl. Ceram. Technol.*, vol. 19, pp. 268–280, 2022, doi: 10.1111/ijac.13915.

[49] A. Bürger, R. van Nieuwenhoven, and I.C. Gebeshuber, "Wings of Death-Mechanical Bactericide by Biomimetics of the Nanopillars on Insect Wings," abstract for poster presented at the *EuroNanoForum 2021*, *Nanotechnology and Advanced Materials for innovation, competitiveness, and sustainability in Europe*, International Iberian Nanotechnology Laboratory, Portugal, 2021.

[50] R. Doh, J. Kim, N. Nam, S. Shin, J. Lim, and J. Shim, "Evaluation of Dimensional Changes during Postcuring of a Three-Dimensionally Printed Denture Base According to the Curing Time and the Time of Removal of the Support Structure: An In Vitro Study," *Appl. Sci.*, vol. 11, no. 21, p. 10000, 2021, doi: 10.3390/app112110000.

[51] M. Ugur, H. Kılıç, M. Berkem, and A. Güngör, "Synthesis by UV-curing and characterisation of polyurethane acrylate-lithium salts-based polymer electrolytes in lithium batteries," *Chem. Pap.*, vol. 68, no. 11, pp. 1561–1572, 2014, doi: 10.2478/s11696-014-0611-1.

[52] Q. Gao, H. Li, and X. Zeng, "Preparation and characterization of UV-curable hyperbranched polyurethane acrylate," *J. Coat. Technol. Res.*, vol. 8, no. 1, pp. 61–66, 2011, doi: 10.1007/s11998-010-9285-y.

[53] A. Herrera-González, M. Caldera-Villalobos, A. Pérez-Mondragón, C. Cuevas-Suárez, and J. González-López, "Analysis of Double Bond Conversion of Photopolymerizable Monomers by FTIR–ATR Spectroscopy," *J. Chem. Educ.*, vol. 96, pp. 1786–1789, 2019, doi: 10.1021/acs.jchemed.8b00659.

[54] B. Mojet, S. Ebbesen, and L. Lefferts, "Light at the interface: the potential of attenuated total reflection infrared spectroscopy for understanding heterogeneous catalysis in water," *R. Chem. Soc. Rev.*, vol. 39, pp. 4643–4655, 2010, doi: 10.1039/c0cs00014k.

[55] M. Palenica, "Functional transformation of Fourier-transform mid-infrared spectrum for improving spectral specificity by simple algorithm based on wavelet-like functions," *J. Adv. Res.*, vol. 14, pp. 53–62, 2018, doi: 10.1016/j.jare.2018.05.009.

[56] R. Simić, J. Mandal, K. Zhang, and N. Spencer, "Oxygen inhibition of free-radical polymerization is the dominant mechanism behind the "mold effect" on hydrogels," *Soft Matter*, vol. 17, pp. 6349-1–6349-10, 2021, doi: 10.1039/d1sm00395j.

[57] A. O'Brien and C. Bowman, "Impact of Oxygen on Photopolymerization Kinetics and Polymer Structure," *Macromolecules*, vol. 39, no. 7, pp. 2501–2506, 2006, doi: 10.1021/ma051863l.

[58] Z. Zhao, X. Mu, J. Wu, H. Qi, and D. Fang, "Effects of oxygen on interfacial strength of incremental forming of materials by photopolymerization," *Extreme Mech. Lett.*, vol. 9, pp. 108–118, 2016, doi: 10.1016/j.eml.2016.05.012.

[59] L. Zhang, C. Wu, K. Jung, Y. Ng, and C. Boyer, "An Oxygen Paradox: Catalytic Use of Oxygen in Radical Photopolymerization," *Angew. Chem. Int. Edit.*, vol. 58, pp 16811–16814, 2019, doi: 10.1002/anie.201909014.